Carbohydrate Polymer Technologies and Applications 2 (2021) 100104

Contents lists available at ScienceDirect

Carbohydrate Polymer Technologies and Applications

journal homepage: www.sciencedirect.com/journal/carbohydrate-polymer-technologies-and-applications

Fluorescent chitosan-based nanohydrogels and encapsulation of gadolinium MRI contrast agent for magneto-optical imaging

Juliette Moreau [a,*], Maité Callewaert [a,*], Volodymyr Malytskyi [a], Céline Henoumont [b], Sorina N. Voicu [c,d], Miruna S. Stan [c], Michael Molinari [e], Cyril Cadiou [a], Sophie Laurent [b,f], Françoise Chuburu [a,*]

[a] Institut de Chimie Moléculaire de Reims, CNRS UMR 7312, University of Reims Champagne-Ardenne URCA, 51685, Reims Cedex 2, France
[b] NMR and Molecular Imaging Laboratory, University of Mons, UMons, B-7000, Mons, Belgium
[c] Faculty of Biology, Department of Biochemistry and Molecular Biology, University of Bucharest, Bucharest, Romania
[d] Faculty of Pharmacy, Department of Pharmacy, Titu Maiorescu University, Bucharest, Romania
[e] CBMN CNRS UMR 5248, University of Bordeaux, INP Bordeaux, 33600, Pessac, France
[f] Center for Microscopy and Molecular Imaging, Rue Adrienne Bolland 8, B-6041, Charleroi, Belgium

A B S T R A C T

In the field of medical imaging, multimodal nanoparticles combining complementary imaging modalities can give rise to new forms of imaging techniques that are able to make diagnosis more precise and confident. In this context, resolution and sensitivity have often to be gathered into a single imaging probe, by combination of MRI and optical imaging for instance. Gadolinium chelate (Gd-CAs) loaded nanohydrogels, obtained from chitosan (CS) and hyaluronic acid (HA) matrix, have shown their efficiency to greatly improve MRI contrast ($r_1 \geq 80$ mM^{-1} s^{-1}). In this study, nanohydrogels were made intrinsically fluorescent by chitosan pre-functionalization and a series of fluorescent chitosans were obtained by covalent grafting of rhodamine (Rhod: 6.3μM) or fluorescein (Fluo: 7.3μM) tags. By combining DOSY and fluorescence data, fluorescent chitosans (CS-Rhod and CS-Fluo) with a low degree of substitution were then selected and used to encapsulate high gadolinium loadings to obtain efficient magneto-optical nanohydrogels.

1. Introduction

Because of its excellent resolution and the absence of patient exposition to ionizing radiations, MRI plays a central role in the arsenal of imaging techniques available to radiologists. This technique is recognized for its excellent resolution but suffers from a lack of sensitivity and information obtained from a simple unenhanced MR image is often not sufficient to highlight the areas of interest in tissues. Usually, this drawback is compensated by the injection of paramagnetic substances, in practice gadolinium chelates GdCAs (such as gadoteric acid also known as DOTAREM®) at high concentration > 0.1 mmol mL^{-1}, whose role is to selectively highlight abnormal tissues by shortening the longitudinal relaxation times of water protons in these tissues (Merbach, Helm & Toth, 2013). Until recently, GdCAs were considered as safe but since the incidence of nephrogenic systemic fibrosis (NSF disease) in patients with unpaired renal function (Rogosnitzky & Branch, 2016) and the observation of MRI brain abnormalities, even with patients with normal renal function (Kanda et al., 2016), the problem is now quite different. Elemental analyses of tissues collected after autopsy of animal models have shown that these manifestations are correlated to *in vivo* Gd demetallation, favored by the lack of chemical inertia of certain GdCAs (of linear structure, that have been since withdrawn from the market) (Gianolio et al., 2017). However, there is currently no clinically available alternative to injecting GdCA during MRI examinations, when it is necessary (Gupta et al., 2020). The alternative is then needed to improve the efficacy of low-risk GdCA to enhance the MRI signal. It is also important to keep in mind that even if MRI provides images with an excellent resolution, it suffers from low sensitivity detection.

A solution is to take advantage of nanoparticle strategy, not only to boost the intrinsic efficacy of GdCAs (defined by their relaxivity r_1 in mM^{-1} s^{-1}) and to convert them into hypersensitive MRI probes, but also to add an optical imaging modality by introduction of fluorophores in the nanoassembly. We have demonstrated that the confinement of a low-risk GdCA such as HGdDOTA (Gadolinium(III)-1.4.7.10-Tetraazacyclododecane-1.4.7.10-tetraacetate, which is the active substance of DOTAREM®) into a nanogel (NG) matrix constituted with polysaccharide biopolymers such as chitosan CS and hyaluronic acid HA (Courant at al., 2012; Callewaert et al., 2014) can provide an interesting alternative to

* Corresponding authors.
E-mail addresses: juliette.moreau@univ-reims.fr (J. Moreau), maite.callewaert@univ-reims.fr (M. Callewaert), francoise.chuburu@univ-reims.fr (F. Chuburu).

https://doi.org/10.1016/j.carpta.2021.100104
Received 6 April 2021; Received in revised form 8 June 2021; Accepted 22 June 2021
Available online 24 June 2021

greatly increase the MRI efficacy of GdCAs. Not only do they have the advantage over types of nanogels (Lux et al., 2013; Soleimani et al., 2013) to overcome the sensitivity disadvantage of Gd contrast agents (Washner et al., 2019) but they are also biocompatible with a low toxicity which is of particular interest for biomedical applications.

Nanogels are water-rich nanoparticles, which is essential to exalt the MRI effect. The question is therefore to know if it is possible to make them fluorescent, without the light emission being reduced. Indeed, their emission may be quenched due to both the high concentration of water OH vibrators (Mei et al., 2021) and metal ions in paramagnetic GdCAs (Asberg et al., 2004) within the nanogels. These nanogels can be made fluorescent by polymer pre-functionalization. In this work, we have chosen to make theses nanogels fluorescent by CS pre-functionalization. CS backbone was modified at the primary amino group of the deacetylated CS units (at C-2, Scheme 1) with rhodamine (Rhod) or fluorescein (Fluo) moieties. For that, we have taken advantage of the higher reactivity of the electronic lone pair of CS primary amino group to graft rhodamine or fluorescein isothiocyanates (RBITC and FITC respectively) *via* a thiourea linkage. Our objective being to involve those fluorescent CS in ionic gelation, it is mandatory to control CS degree of substitution (DS_{CS}) after functionalization. Indeed, sufficient remaining positive charges are necessary on fluorescent CS backbone to perform subsequent ionic gelation with HA in the presence of an ionogenic cross linker (Gupta & Jabrail, 2006; Sang et al., 2020). Therefore, CS functionalization with rhodamine and fluorescein has to be carefully characterized, especially in the absence of an unambiguous marker of the thiourea bond (Ma et al., 2008). In this context, a series of CS-fluorophore conjugates (CS-Rhod or CS-Fluo conjugates) were synthesized in which the level of Rhod or Fluo substitution was systematically varied and quantified by a combination of fluorescence and DOSY experiments. CS-fluorophores conjugates were then involved in nanogel synthesis in the presence of GdCAs and after detailed morphological and toxicological characterizations, the efficacy of the corresponding fluorescent Gd nanogels as potential magneto-optical nanoprobes was explored.

2. Materials and Methods

2.1. Materials

Chitosan (CS, from shrimp shells, 51 kDa, viscosity = 33mPa.s in 1% acetic acid, 20°C) was purchased from Sigma-Aldrich. A deacetylation degree (DD) of 86% was determined by ^{1}H NMR spectroscopy according to published procedures. (Hirai et al., 1991; Vårum et al., 1991) For calculations, CS repetitive unit (rep unit) molecular mass in which CS DD was taken into account, was considered to be M_W in average ($CS_{rep\ unit}$) = 200 g.mol^{-1} (Courant et al., 2012). Hyaluronic acid sodium salt (HA 1000 kDa extracted from *Streptoccus equi sp*), Rhodamine B isothiocyanate (RBITC, No. R1755), Fluorescein isothiocyanate (FITC), acetic acid and sodium acetate were purchased from Sigma-Aldrich. Sodium tripolyphosphate (TPP) was purchased from Acros Organics. DCl (35 wt % in D_2O) and D_2O were provided from Sigma-Aldrich and Euriso-top, respectively. HGdDOTA (Gadolinium(III)-1.4.7.10-Tetraazacyclododecane-1.4.7.10-tetraacetate) was synthesized according a published procedure (Courant et al., 2012).

Fetal bovine serum (FBS), heat inactivated was purchased from Gibco by Life Technologies (New Zealand), Roswell Park Memorial Institute (RPMI) 1640 medium and Dulbecco's Modified Eagle's Medium (DMEM) from Gibco (Invitrogen, Grand Island, N.Y., USA), 3-(4,5-dimethylthiazol-2-yl)-2,5-diphenyltetrazolium bromide (MTT), *In Vitro* Toxicology Assay Kit Lactic Dehydrogenase based and antibiotics (penicillin, streptomycin and amphotericin B) were provided by Sigma-Aldrich (St. Louis, MO, USA). Sterile water for injections (Laboratoire Aguettant, Lyon, France) was systematically used for polymer, nanoparticle preparations and analyses.

All products were used as received, without further purification.

Native and functionalized polymers (CS, CS-Rhodamine namely CS-Rhod and CS-Fluorescein namely CS-Fluo, respectively) were characterized by FTIR (Nicolet IS 5 spectrometer equipped with an ATR ID5 module), ^{1}H NMR (Bruker Avance III 500 MHz NMR spectrometer) at 318 K with D_2O/DCl (700/1, v/v) as solvent, UV-visible and fluorescence spectroscopies (Varian Cary 5000 Shimadzu UV-2401PC and Varian Cary Eclipse, respectively). Centrifugation experiments were performed with an Alegra X-30 centrifuge (Beckman-Coulter).

The diffusion coefficients of different materials (CS, RBITC, FITC, CS-Rhod and CS-Fluo) were determined by DOSY experiments (Diffusion Ordered SpectroscopY) on a Bruker Avance II 500 MHz NMR spectrometer.

2.2. Preparation, IR and ^{1}H NMR characterizations of CS-Rhodamine and CS-Fluorescein polymers

2.2.1. CS-Rhodamine (CS-Rhod) synthesis

CS (200 mg, 1.0 mmol of NH_2 function) was dissolved under N_2 atmosphere in 10 mL of an aqueous solution of acetic acid 1% (v/v). After complete CS dissolution, the pH was adjusted to 5 by addition of 1M NaOH and 5 mL of MeOH was added and the resulting solution allowed to stir for 3h (Ma et al., 2008). Then, different stoichiometric ratios of RBITC were added in anhydrous MeOH to the CS solution (RBITC/NH_2 CS molar ratio expressed as % mol $(NCS/NH_2)_{initial}$ of 2, 5 and 10%, corresponding to 11, 27 and 53 mg of RBITC in 3.5, 8 and 16 mL of anhydrous MeOH respectively). The RBITC solution was added dropwise to the CS solution and the mixture was stirred under N_2 atmosphere, in the dark at room temperature for 36h. At the end of the reaction, CS-Rhod was precipitated by using a NaOH solution (1M), and the resulting precipitate washed with water for injection. The polymer was recovered by centrifugation (6500 rpm, 12 min, at room temperature) and the overall procedure repeated until waste water reached pH 7 and no fluorescence being detected in the corresponding solution. CS-Rhod was finally obtained after freeze-drying as a pink-mauve foam (between 120 and 180 mg according to the sample).

FT-IR (ATR, cm^{-1}): 3362 (ν_{OH} and ν_{NH}), 2871 (ν_{CH}), 1650 (amide I), 1559 (amide II), 1053, 1027 (pyranose ring).

^{1}H NMR (500 MHz, 318K, D_2O/DCl: 700 µL/1µL), δ (ppm): 1.30 (t, CH_3 - Rhod), 2.07 (s, CH_3 - CS acetyl units), 2.99 (s, 1H, CS), 3.37 (s, CH_2 - Rhod), 3.5-4.2 (m, 5H, CS), 4.71 (s, 1H, CS), 6.9-7.9 (aromatic H - Rhod).

2.2.2. CS-Fluorescein (CS-Fluo) synthesis

CS-Fluorescein (CS-Fluo) was synthesized according to the same procedure, *i.e.* from a CS solution (mixture of acetic acid and anhydrous MeOH) and FITC solution (in anhydrous MeOH). The same FITC/NH_2 CS molar ratios were prepared namely 2, 5 and 10% (expressed as % mol $(NCS/NH_2)_{initial}$) corresponding to 8, 20 and 40 mg of FITC in 3, 7.5 and 15 mL of anhydrous MeOH respectively.

After precipitation (with 1 M NaOH) and washing with water for injection until pH 7, CS-Fluo was finally obtained after freeze-drying as an orange foam (between 130 and 180 mg according to the sample).

FT-IR (ATR, cm^{-1}): 3288 (ν_{OH} and ν_{NH}), 2874 (ν_{CH}), 1634 (amide I), 1573 (amide II), 1063, 1028 (pyranose ring).

^{1}H NMR (500 MHz, 318K, D_2O/DCl: 700 µL/1µL), δ (ppm): 2.07 (s, CH_3 - CS acetyl units), 3.02 (s, 1H, CS), 3.5-4.2 (m, 5H, CS), 4.73 (s, 1H, CS), 6.5-8.0 (aromatic H - Fluo).

2.3. Determination of CS degree of substitution (DS_{CS}) by a combination of fluorescence and DOSY experiments

In order to determine the degree of substitution of chitosan in CS-Rhod (DS_{CS}^{Rhod}) or CS-Fluo (DS_{CS}^{Fluo}) samples, it was mandatory to distinguish between the grafted amount of fluorophore ($RBITC_G$ namely $Rhod_G$ or $FITC_G$ namely $Fluo_G$) and the ungrafted one ($Rhod_{UG}$ or

$Fluo_{UG}$). For that, a combination of fluorescence spectroscopy and DOSY experiments was applied.

Fluorescence spectroscopy: The total amount of fluorophore ($Rhod_T$ or $Fluo_T$) which corresponded to the sum of the grafted fluorophore amount ($Rhod_G$ or $Fluo_G$) and the ungrafted one ($Rhod_{UG}$ or $Fluo_{UG}$), was determined by fluorescence spectroscopy after sample purification. For this purpose, we measured the emission intensities at 576 nm (rhodamine) or 511 nm (fluorescein) of 0.25-0.45 mg mL^{-1} solutions of CS-Rhod (or CS-Fluo), dissolved in an aqueous solution of acetic acid 1% (v/v) and diluted 100 times with acetate buffer (pH 4.7) (Varian Cary Eclipse spectrometer, with $\lambda_{exc} = 550$ and 450 nm for rhodamine and fluorescein emission measurements respectively, and $\Delta\lambda_{exc} = \Delta\lambda_{em} = 5$ nm). The ratio of the total amount of fluorophore to chitosan (fluorophore$_T$/ CS) was calculated as the percent molar concentration of fluorophore to CS molar concentration according to Eq. 1.

$$\%\left(\frac{fluorophore_T}{CS}\right)_{mol} = \frac{I_{fluorophore}/k_{fluorophore}}{m_{CS-fluorophore}/(M_{CS_{rep\ unit}} \times V)} \times 100 \quad (1)$$

with $I_{fluorophore}$ being the emission intensity measured at 576 and 511 nm for CS-Rhod and CS-Fluo respectively, $k_{fluorophore}$ being equal to the ratio between the emission intensity (at 576 or 511 nm) and the fluorophore concentration. $k_{fluorophore}$ was determined for rhodamine and fluoresceine by calibration with standard solutions of each fluorophore. Serial dilutions in acetate buffer (pH 4.7) of a stock methanolic solution of each fluorophore (150 mg mL^{-1}) were prepared to reach fluorophore concentrations ranging from 0.003 to 0.1 mg mL^{-1}. The corresponding proportionality coefficient determined were $k_{Rhod,\ 576\ nm} = 1.75 \times 10^9$ $mol^{-1}L$ and $k_{Fluo,\ 511\ nm} = 4.58 \times 10^8$ $mol^{-1}L$.

DOSY Experiments: Due to the large difference between rhodamine (or fluorescein)and CS-Rhod (or CS-Fluo) molecular weights, it was expected to discriminate between ungrafted and grafted fluorophore, using their respective diffusion coefficients. For that, preliminary DOSY experiments were performed to determine CS, rhodamine (Rhod) and fluorescein (Fluo) diffusion coefficients (D_{CS}, D_{Rhod} and D_{Fluo} respectively). Bipolar gradient pulses with two spoil gradients were used to measure these coefficients (BPP-LED pulse sequence). The value of the gradient pulse length τ was 4 ms for CS and 2ms for Rhod and Fluo, while the value of the diffusion time Δ was set to 500 ms for CS and 250 ms for Rhod and Fluo. The pulse gradients were incremented in 16 steps from 2% to 95% of the maximum gradient strength (53.5 G/cm) in a linear ramp and the temperature was set at 30°C. CS, Rhod and Fluo diffusion curves were then extracted from DOSY spectra of CS (for the peak at $\delta = 2.1$ ppm), Rhod (for the peak at $\delta = 1.2$ ppm) and Fluo (for the peak at $\delta = 6.8$ ppm). In each case, the mono-exponential diffusion curves were fitted with Eq. 2 (Johnson, 1999; Augé, Amblard-Blondel & Delsuc, 1999) to obtain D_{CS} value of 5×10^{-12} m^2s^{-1}, and D_{Rhod} and D_{Fluo} values of 2×10^{-10} m^2s^{-1} and 4×10^{-10} m^2s^{-1} respectively (Figure S4).

$$I = I_o exp\left[-\gamma^2 g^2 D\delta^2(\Delta - (\delta/3) - (\tau/2))\right] \quad (2)$$

Then, similar DOSY experiments were performed with CS-Rhod and CS-Fluo. The diffusion curves were extracted from CS-Rhod and CS-Fluo DOSY spectra, for the more intense peak of Rhod and Fluo, at 1.3 and 6.8 ppm respectively. The diffusion curves that showed a monoexponential evolution were fitted according to Eq. 2. The diffusion curves that exhibited a biexponential evolution were fitted according to Eq. 3, (Johnson, 1999; Augé, Amblard-Blondel & Delsuc, 1999)

$$I = I_G exp\left[-\gamma^2 g^2 D_G \delta^2(\Delta - (\delta/3) - (\tau/2))\right] + I_{UG} exp\left[-\gamma^2 g^2 D_{UG} \delta^2(\Delta - (\delta/3) - (\tau/2))\right] \quad (3)$$

where I_G and I_{UG} were the intensities at 0% gradient, for grafted and ungrafted fluorophore (Rhod or Fluo) respectively, γ the gyromagnetic ratio, g the gradient strength, D_G and D_{UG} the diffusion coefficients of grafted and ungrafted fluorophores respectively, δ the gradient pulse length, Δ the diffusion time and τ the interpulse spacing in the BPP-LED pulse sequence.

During the fitting, D_G and D_{UG} were then fixed to values measured independently on chitosan and rhodamine or fluorescein, respectively: $D_{CS} = 5 \times 10^{-12}$ m^2s^{-1}, $D_{Rhod} = 2 \times 10^{-10}$ m^2s^{-1} and $D_{Fluo} = 4 \times 10^{-10}$ m^2s^{-1}.

I_G and I_{UG} values extracted from the fitting, allowed to calculate the percentage of grafted fluorophore over the total amount of fluorophore (fluorophore$_G$/fluorophore$_T$) (Eq. 4):

$$\%\frac{Fluorophore_G}{Fluorophore_T} = \frac{I_G}{I_G + I_{UG}} \times 100 \quad (4)$$

The percentage of fluorophore grafted to CS chains (DS_{CS}) was then calculated Eq. 5) from emission measurements and DOSY experiments (from Eqs. 1 and (4):

$$DS_{CS} = \%\left(\frac{fluorophore_G}{CS}\right) = \frac{I_{fluorophore}/k_{fluorophore}}{m_{CS-fluorophore}/(M_{CS_{rep\ unit}} \times V)} \times \frac{I_G}{I_G + I_{UG}} \times 100 \quad (5)$$

where I_G and I_{UG} stand for the intensities extracted from the DOSY experiments, for grafted and ungrafted fluorophores (rhodamine or fluorescein) respectively.

2.4. Preparation and characterization of CS−Rhod and CS-Fluo nanoparticles by ionic gelation (CS−Rhod-TPP/HA and CS−Fluo-TPP/HA nanogels)

2.4.1. CS−Rhod-TPP/HA and CS−Fluo-TPP/HA nanogel syntheses

Solutions of fluorescent CS were prepared by dissolution of CS-Rhod (DS_{CS}^{Rhod} = 0.85%) or CS-Fluo (DS_{CS}^{Fluo} = 0.86%) powders in citric acid (10% wt/v) solutions (2.5 mg mL^{-1}).

CS-fluorophore-TPP/HA nanogels (CS−Rhod-TPP/HA and CS−Fluo-TPP/HA NGs) were obtained by an ionotropic gelation process. For this purpose, the polyanionic aqueous phase (4.5 mL) containing both HA (0.8 mg mL^{-1}) and TPP (1.2 mg mL^{-1}) was added dropwise to the CS-fluorophore solution (9 mL) under sonication (750W, amplitude 32%). At the end of the addition, magnetic stirring was maintained for 10 min. Purification and pH correction of the nanosuspensions was then carried out by dialysis against water for injection (3 × 12h) using a membrane of 25 kDa cut-off (Spectrum Lab) to reach physiological pH. Gadolinium-loaded nanogels (GdDOTA⊂CS-Rhod-TPP/HA and GdDOTA⊂CS-Fluo-TPP/HA NGs) were prepared in the same way, by incorporating HGdDOTA (17 mg) as the MRI contrast agent in the anionic phase.

2.4.2. CS−Rhod and CS−Fluo nanogels characterization by Dynamic Light Scattering

The nanogels averaged hydrodynamic diameters (Z-ave) were determined by Dynamic Light Scattering (DLS) with a Zetasizer Nano ZS (Malvern Zetasizer Nano-ZS, Malvern Instruments, Worcestershire, UK). Each sample was analyzed in triplicate at 20°C at a scattering angle of 173°, after a 1/20 dilution in water. Water was used as a reference dispersing medium.

ζ-(zeta) potential data were collected through Electrophoretic Light Scattering (ELS) at 20°C, 150 V, in triplicate for each sample, after a 1/20 dilution in water. The instrument was calibrated with a Malvern – 68 mV standard before each analysis cycle.

2.4.3. In vitro cytotoxicity of CS-Rhod and CS-Fluo nanogels

RAW 267.4 and A20 cell lines were purchased from American Type Culture Collection (ATCC catalog no., TIB-7 and TIB-208, respectively). RAW 267.4 cells (adherent cells) were cultured in Dulbecco Modified Eagle Medium (DMEM) pH 7.4 with 4 mM L-glutamine adjusted to contain 4.5 g L^{-1} glucose and, 1.5 g L^{-1} sodium bicarbonate. The growth

medium was supplemented with 10% fetal bovine serum, 1% antibiotics (penicillin, streptomycin, amphotericin). The A20 cell line (murine B lymphocytes, from reticulum cell sarcoma in suspension) were cultured in RPMI 1640 medium pH 7.4 with 2 mM L-glutamine, 1.5 g L^{-1} Na_2CO_3, 4.5 g L^{-1} glucose, 1 mM sodium pyruvate, 10 mM HEPES and supplemented with 10% fetal bovine serum and 1% antibiotics (penicillin, streptomycin, and amphotericin). All cell types were maintained at 37°C in a humidified atmosphere (95%) with 5% CO_2. The concentration of CS-Rhod-TPP/HA and CS-Fluo-TPP/HA stock nanosuspensions was 1.17 mg mL^{-1} and the Gd concentration of GdDOTA⊂CS-Rhod-TPP/HA and GdDOTA⊂CS-Fluo-TPP/HA stock nanosuspensions was 0.144 mM and 0.144 mM respectively. Dilutions were then made in the culture medium for each cell line tested. In parallel, the cells seeded in 24-well plates at a density of 10^5 cells mL^{-1} for RAW 264.7 and 2×10^5 cells mL^{-1} for A20 cell lines, were incubated for 6 and 24 hours at different concentrations of CS-Rhod-TPP/HA, CS-Fluo-TPP/HA nanogels (*i.e.* 5, 15, 30, 60 and 120 μg mL^{-1}) or GdDOTA⊂CS-Rhod-TPP/HA and GdDOTA⊂CS-Fluo-TPP/HA nanogels (*i.e.* 0.5, 1, 2.5, 5 and 10 μM of Gd).

Cell viability was measured by the MTT, 3-(4,5-dimethylthazol-2-yl)-2,5-diphenyl tetrazolium bromide), assay**.** After the exposure time, the culture medium was removed and in each well were added 500 μL MTT (1 mg mL^{-1}) for 2 hours. After that, the MTT solution was removed and the formazan crystals were solubilized in 100% isopropanol. The optical density was measured at 595 nm using Flex Station 3 Multi-Mode Microplate Reader. The cell viability was expressed in percentage considering 100% viability for control cells.

The LDH release was measured in the culture media of treated cells using the *In Vitro* Toxicology Assay Kit (Sigma-Aldrich, USA) and compared to the LDH release level of control (untreated cells). After each exposure interval, a volume of 50 μL medium was taken from each sample and placed on a 96-well microtiter plate and then 100 μL of assay mixture were added. After 20-30 min at room temperature, the reaction was stopped by adding 1/10 volume of HCl 1 M and the enzymatic activity was determined spectrophotometrically using the Flex Station 3 Multi-Mode Microplate Reader. The absorbance was read at 450 nm and the results were expressed relative to control.

2.4.4. Fluorescent nanogels characterization by Atomic Force Microscopy (AFM) and confocal microscopy

To obtain information about the different NP sizes and their fluorescent properties, correlative experiments were performed using an Atomic Force Microscope (AFM) coupled to a confocal microscope. Each sample was analyzed in triplicate at 20°C after a 1/20 dilution in water. To be observed, the NPs were deposited on a glass slide and after one hour, the samples were rinsed with deionized water. All the experiments were performed in water to avoid nanogel drying (and thus possible changes in their structures / morphologies).

First a confocal image was acquired using a Axio Observer 7 LSM 800 Airyscan microscope (ZEISS, Germany). For the excitation wavelength, lasers at 561 and 488 nm were used for the CS-Rhod-TPP/HA and CS-Fluo-TPP/HA nanogels, respectively. A 100 × objective was used and 512 pixels × 512 pixels image were acquired. Then in a second time, areas with fluorescent NPs were chosen and scanned with a Resolve AFM (BrukerNano, USA). Peak Force Tapping Quantitative Nano-Mechanicals (PFT-QNM) mode was used to perform AFM imaging of the different samples in liquid conditions. Nitride coated silicon cantilevers (SNL, Bruker probes, USA) with a resonance frequency of 65 kHz, a nominal spring constant of 0.35 N/m and a tip radius of 6 nm were used for this work and were calibrated for each experiment. Images were acquired with a scan rate of ~ 1.0 - 1.5 Hz, with a force kept as low as possible (typically 0.5 nN or lower). Imaging gains were automatically optimized by the software. The different AFM images were analyzed and processed with the Nanoscope Analysis 2.0 software (BrukerNano, USA). At least, 5 different areas for each sample were analyzed by AFM to determine averaged NP diameters.

2.5. Determination of the gadolinium concentration in nanogels by ICP-OES

Gadolinium nanoparticle loading was determined on purified and concentrated nanosuspensions by Inductively Coupled Plasma - Optical Emission Spectroscopy (ICP-OES). The non-encapsulated complexes were separated from the NGs by high speed centrifugation for 1 h 15 min at 4°C and 23 200 g (Beckman Avanti™ J-E Centrifuge, France). The NP pellet was then incubated overnight in a 1:3 (v/v) mixture of HCl (37%) and HNO_3 (69%) in order to release Gd from the polymer matrix and the complexes. After the NG destruction, volumetric dilutions were carried out to achieve an appropriate Gd concentration within the detection range of the method. Similar procedure was implemented to determine Gd content in supernatants. Samples were analyzed using ICAP 6000 series ICP-OES spectrometer. Counts of Gd were correlated to a Gd calibration curve generated by mixing $Gd(NO_3)_3$ standard with unloaded NGs incubated under the same acidic conditions.

2.6. Evaluation of fluorophore concentration in nanogels by fluorescence spectroscopy

Rhodamine or fluorescein concentrations were determined by fluorescence (Varian Cary Eclipse spectrometer) on dialysed nanogels, after high speed centrifugation (23 200 g, 1 h 15, 4°C) both in NP pellets and in supernatants, using the same methodology as the one used for the determination of fluorophore concentrations on CS-Rhod and CS-Fluo polymers.

2.7. Relaxivity measurements

NMRD profiles. ^{1}H NMRD profiles were measured on a Stelar Spinmaster FFC fast field cycling NMR relaxometer (Stelar, Mede, Pavia, Italy) over a range of magnetic fields extending from 0.24 mT to 0.7 T and corresponding to ^{1}H Larmor frequencies from 0.01 to 30 MHz using 0.6 mL samples in 10 mm o.d. tubes. The temperature was kept constant at 37°C. An additional relaxation rate at 60 MHz was obtained with a Bruker Minispec mq60 spectrometer (Bruker, Karlsruhe, Germany). The diamagnetic contribution of unloaded particles was measured and subtracted from the observed relaxation rates of the Gd-loaded nanoparticles.

MR Imaging. MR imaging of NP suspensions were performed using a 3.0 T MRI device (Skyra, Siemens Healthcare, Erlangen, Germany) with a 15 channel transmit/receive knee coil. T_1-weighted images were obtained with an 3D fast spin-echo T_1 sequence (TR = 700 ms, TE = 12 ms, FOV = 201 × 201 mm, matrix= 256 × 256, voxel size = 0.78 × 0.78 × 2mm). T_2-weighted images were obtained with an 3D fast spin-echo T_2 sequence (TR = 1000 ms, TE = 103 ms, FOV = 199 × 199 mm, matrix = 384 × 384, voxel size = 0.52 × 0.52 × 0.55mm). The gadolinium concentrations were tested in the 25–200 μM range.

3. Results and Discussion

3.1. Preparation and characterization of CS grafted with Rhodamine B Isothiocyanate (CS-Rhod) and Fluorescein Isothiocyanate (CS-Fluo)

The functionalization of chitosan (CS) by conventional fluorophores, namely RBITC and FITC that emitted in red and green regions respectively, was performed by a direct coupling between the fluorophore isothiocyanate group and the amino function of the CS glucosamine residue. (Ma et al., 2008) To optimize the labelling procedure, several initial molar ratios (NCS/NH_2), chosen between 2 and 10% for each fluorophore, were used in order to provide sufficient grafting yields while avoiding optical signal saturation. After workup and freeze-drying, fluorescent CS samples were characterized by UV-visible and emission spectroscopies, FT-IR and ^{1}H NMR at 318 K (D_2O/DCl as solvent). The absorption and fluorescence maxima in water medium of

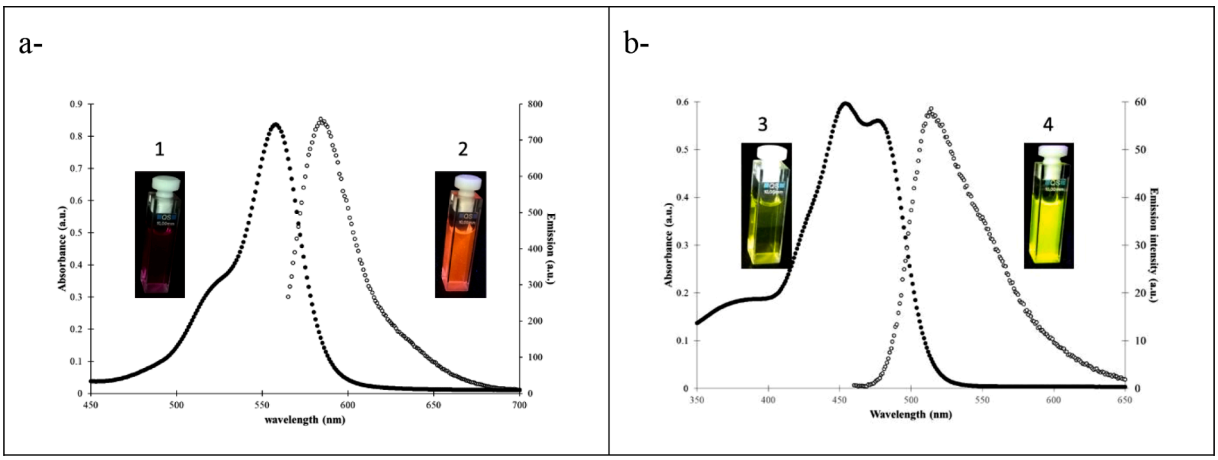

Figure 1. Absorbance (●) and emission (○) spectra of in acetate buffer (pH 4.7), (a) CS-Rhod; (b) CS-Fluo, % mol $(NCS/NH_2)_{initial} = 10\%$. Optical images of CS-Rhod and CS-Fluo under natural light (pictures 1 and 3, respectively) and under UV light (365 nm, pictures 2 and 4, respectively).

CS-Rhod were located at 550 nm and 576 nm, respectively, and the ones of CS-Fluo were located at 450 nm and 511 nm, respectively (Figure 1). They were similar to those of the free dyes (Leng et al., 2017; Xia et al., 2016). FT-IR spectra of CS-Rhod and CS-Fluo samples (Figure S1) showed the disappearance of the FT-IR band at 2030-2150 cm^{-1} attributed to the isothiocyanate group (Sinagaglia et al., 2012). These data suggested the involvement of the thiourea moiety in the conjugation of both fluorophores with CS.

Similarly, ^1H NMR spectra of CS-Rhod and CS-Fluo (Figure S2), in addition to chemical shifts corresponding to CS backbone or acetyl protons (H_2 of pyranose ring at $\delta = 3.0$ ppm, H_3 to H_6 of pyranose ring at $\delta = 3.5$-4.2 ppm, anomeric H_1 at $\delta = 4.7$ ppm and acetyl protons at $\delta = 2.1$ ppm), confirmed the presence of rhodamine moiety in CS-Rhod samples (Figure S2a - H_a at $\delta = 1.3$ ppm, H_b at $\delta = 3.4$ ppm, and H_{ar} at $\delta = 6.9$-7.9 ppm) as well as fluorescein moiety in CS-Fluo samples (Figure S2b - H_{ar} at $\delta = 6.5$-8.0 ppm).

In the absence of a spectroscopic marker specific to the thiourea linkage, the evaluation of CS degree of substitution (DS_{CS}) post-grafting, cannot be given by the sole ^1H NMR spectra analyses since they only help to determine the total amount of fluorophore associated to CS. Indeed, in CS-Rhod samples this amount ($Rhod_T$) could be determined by the ratio between the integration of H_a rhodamine ^1H signal (divided by 12) and chitosan signals (H_2 CS ^1H signal which was set to 1). Similar analysis could be performed for CS-Fluo, the total amount of fluorescein associated to CS ($Fluo_T$) being obtained *via* the ratio between the integration of fluorescein aromatic ^1H (divided by 9) and chitosan signals (H_2 CS ^1H signal always set to 1). Unfortunately for the lowest initial (NCS/NH_2) molar ratio (2%), the ^1H signals associated to each fluorophore were too weak to be integrated with accuracy. To circumvent this drawback, the total amount of each optical probe was determined by fluorescence and this, for each (NCS/NH_2) initial ratio (*Eq. 1* Experimental Section). The results obtained from fluorescence spectroscopy showed that after workup, the total amount of rhodamine ($Rhod_T$) associated to CS were 0.18, 0.44 and 1.03% for (NCS/NH_2) initial ratios of 2, 5 and 10%, respectively (Table S3), the total amount of fluorescein ($Fluo_T$) associated to CS being 0.22, 0.54 and 1.02% for the same (NCS/NH_2) initial ratios, respectively. These data indicated then that only 10% of the probe (Rhod or Fluo) initially introduced remained associated to CS after reaction, which highlighted the efficiency of purification step.

In order to properly evaluate the amount of grafted fluorophore ($Rhod_G$ or $Fluo_G$), CS-Rhod and CS-Fluo samples were subjected to DOSY experiments (Belabassi et al., 2017).

In the case of CS-Rhod polymers, these curves extracted from CS-Rhod DOSY spectra were clearly non-linear (Figures 2 a-c). Their biexponential shape highlighted in these samples the presence of two contributions, one coming from the ungrafted rhodamine ($Rhod_{UG}$) which diffused faster than the second one coming from grafted rhodamine to CS chains ($Rhod_G$). Due to first the large difference between rhodamine and CS molecular weights and second taking into account the weak percentages determined by fluorescence of fluorophores associated to the polymer chains (*vide supra*), one can assume that fluorophore grafting should not restrict CS chain mobility and consequently, CS-Rhod molecular weight must be close to the one of CS. Therefore, a bi-exponential fitting of these curves was performed (Eq. 3), for which two diffusion coefficients of 2×10^{-10} m^2 s^{-1} (for $Rhod_{UG}$, Figure S4) and 5×10^{-12} m^2 s^{-1} (for CS, Figure S4 and then CS-Rhod) were used.

In the case of CS-Fluo polymers, the diffusion curves extracted from DOSY spectra were linear for the two first ratios (2 and 5%) and clearly non-linear for the last one (10%) (Figures 2 d-f). For the two first cases, a mono-exponential fitting was considered (Eq. 2) which led to a diffusion coefficient close to the one measured on chitosan alone, meaning that 100 % of the fluorophore present was grafted to chitosan. For the third one, a bi-exponential fitting was performed for which two diffusion coefficients of 4×10^{-10} m^2 s^{-1} (for $Fluo_{UG}$, Figure S4) and 5×10^{-12} m^2 s^{-1} (for CS, Figure S4 and then CS-Fluo) were fixed. Thus, the curves fitting allowed to extract the percentage of grafted fluorophore over their total amount ($Rhod_G/Rhod_T$ and $Fluo_G/Fluo_T$, Eq. 4).

According to the initial molar ratio, $Rhod_G/Rhod_T$ ratios were estimated between 67 and 91 % while $Fluo_G$ / $Fluo_T$ ratios were estimated between 84 and 100 % (Table S3). These results indicated that almost all the fluorophores present in fluorescent CS samples were grafted. Final DS_{CS}, as far as they are concerned, were comprised between 0.16 and 0.86 % (Table S3) whatever the fluorophore. This indicated that at least 1% of amino functions were functionalized with Rhod or Fluo, and that sufficient protonable amino functions remained available to be involved in the preparation of nanoparticles by ionic gelation.

3.2. CS-Rhod-TPP/HA and CS-Fluo-TPP/HA nanogel syntheses and characterizations

CS-Rhod with a DS_{CS} of 0.85% and CS-Fluo with a DS_{CS} of 0.86% were then evaluated for their ability to produce fluorescent CS-Rhod-TPP/HA and CS-Fluo-TPP/HA nanogels able to encapsulate gadolinium chelate. For that, CS-Rhod and CS-Fluo polymers in association with sodium hyaluronate (HA) in the presence of tripolyphosphate (TPP) were used to produce under mild conditions and without the use of solvents except water, nanoparticles by ionic gelation (Scheme 2). These conditions allowed the development of multivalent electrostatic interactions between the polycationic phase constituted of CS derivatives

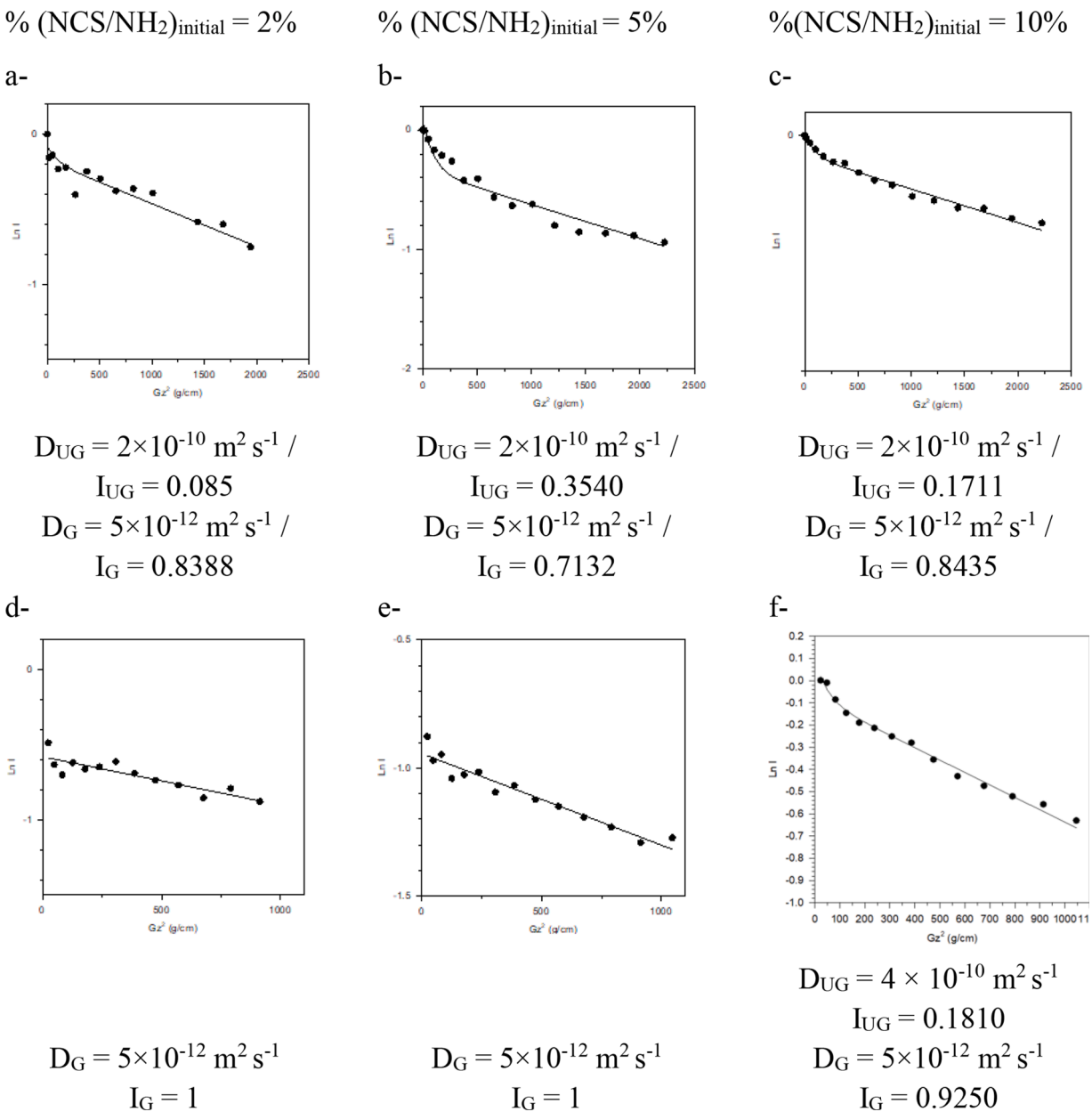

Figure 2. Diffusion curves and diffusion coefficients extracted from DOSY spectra of (a-c) CS-Rhod (for the peak at δ = 1.25 ppm and (d-e) CS-Fluo (for the peak at δ = 6.8 ppm) according to initial (-NCS/CS)l molar ratios

Table 1
Intensity weighted (Z-average) diameters, polydispersity indexes (PdI), zeta potential (ζ) and Gd(III) loadings of CS-Rhod-TPP/HA and CS-Fluo-TPP/HA nanogels

Polymer	Before dialysis Z-ave ± sd (nm)	PdI ± sd	ζ ± sd (mV)	After dialysis Z-ave± sd (nm)	PdI ± sd	ζ ± sd (mV)	d_{AFM}±sd(nm)	$[Gd]_{NP}$ (mM)
CS-Rhod	241 ± 11	0.16 ± 0.02	49 ± 1	321 ± 20	0.22 ± 0.01	38 ± 2	65 ± 13	97
CS-Fluo	195± 10	0.17 ± 0.01	48 ± 1	221± 14	0.24 ± 0.01	35 ± 1	57 ± 10	111
CS	*219 ± 10*	*0.20 ± 0.01*	*43 ± 4*	*226 ± 10*	*0.19 ± 0.01*	*35 ± 1*	*62 ± 12*	*96*

and the polyanionic chains of HA (ionic complexation between these polymers), these polymeric chains being interconnected by the low-molecular weight cross-linker, TPP. (Berger et al., 2004). With each polymer tested, stable and homogeneous nanosuspensions were obtained.

Gadolinium-loaded nanoparticles were prepared in the same way by incorporating HGdDOTA as the MRI contrast agent in the preparation. This macrocyclic gadolinium chelate, characterized by a high thermodynamic and kinetic stability, is the active substance of DOTAREM®. It is recognized as low-risk towards nephrogenic systemic fibrosis (NSF) in renal impaired patients (Khawaja et al., 2015) and its macrocyclic structure helps to prevent gadolinium leakage and subsequent deposition in brain (Gianolio et al., 2017). The resulting GdDOTA⊂CS-Rhod-TPP/HA or GdDOTA⊂CS-Fluo-TPP/HA nanoparticles (Table 1) had similar morphological characteristics as the non-fluorescent ones (Table S5).

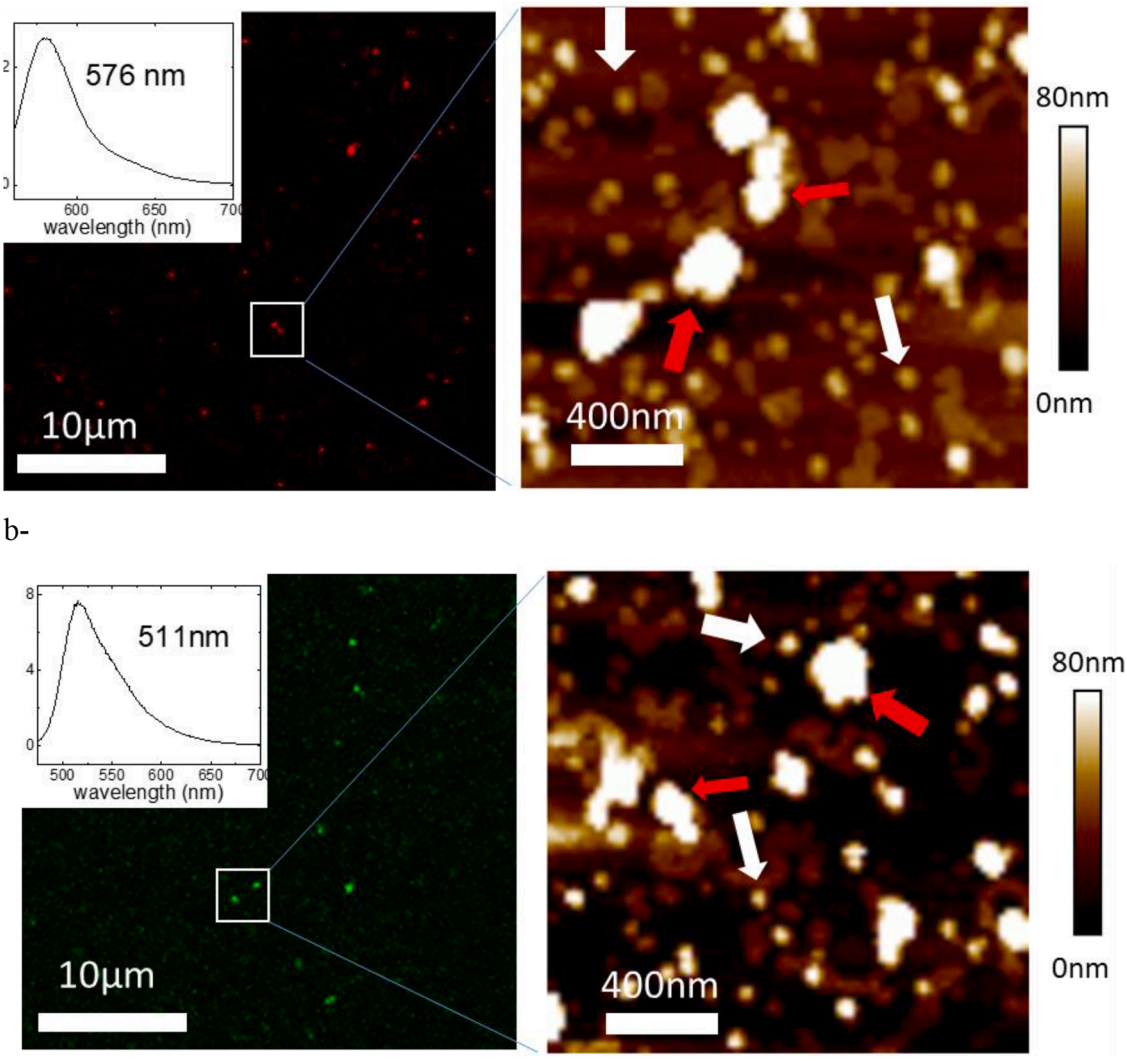

Figure 3. Confocal and associated AFM images of (a) HGdDOTA ⊂ CS-Rhod/HA/TPP NGs, and (b) HGdDOTA ⊂ CS-Fluo/HA/TPP NGs after dialysis.

ICP-OES analyses of GdDOTA⊂CS-Rhod-TPP/HA or GdDOTA⊂CS-Fluo-TPP/HA nanoparticles indicated that their gadolinium loading, around 100 mM, was similar to those of GdDOTA⊂CS-TPP/HA controls (Table 1).

To characterize the morphology and the optical properties of the fluorescent nanohydrogels, confocal images coupled to AFM measurements in liquid were used (Figure 3), thanks to a correlative setup. Compared to other types of microscopies, AFM allows to have a high resolution while keeping the proper physiological environment and then minimal physical perturbations to these fragile samples (which can burn under electronic irradiation for instance). From a methodological point of view, it was possible to check first the fluorescent properties of the NGs through confocal microscopy and then to focus on a proper area to get a morphological characterization of the NGs by AFM. On Figure 3a, the confocal image and the associated fluorescence spectrum with a maximum at 576 nm exhibited the expected features for the HGdDOTA⊂CS-Rhod/HA/TPP NGs, confirming the fact that the NGs are fluorescent. On Figure 3b, the same behavior was found for the HGdDOTA⊂CS-Fluo/HA/TPP NGs with an emission at 511nm.

Zooming with the AFM on a proper area allowed to show that, whatever the nanosuspensions, the NGs were spherical particles and no significant morphological differences could be noticed with a mix of isolated NPs (white arrows) or NG aggregates (red arrows). Whatever the samples (with, or without HGdDOTA), the isolated NG diameters calculated from the AFM images were inferior to 100 nm typically in the range of 60 nm (see Tables 1 and S5) and the aggregates from 150 to 400 nm. Regarding the confocal images, the brighter and larger spots could be attributed to the aggregates. As for the comparison with the DLS measurements, such differences have already been observed for nanogels and could be attributed to the fact that in DLS, because of the presence of aggregates, the response could be biased by the use of mathematical models of signal processing (Rigaux et al., 2017).

Rhod and Fluo concentrations associated with nanogels were then determined by fluorescence. Rhod and Fluo concentrations associated with GdDOTA⊂CS-Rhod-TPP/HA or GdDOTA⊂CS-Fluo-TPP/HA NGs were 6.3 and 7.3 µM respectively. Furthermore, emission spectra of GdDOTA⊂CS-Rhod-TPP/HA or GdDOTA⊂CS-Fluo-TPP/HA nanosuspensions were superimposable to those of unloaded CS-Rhod-TPP/HA or CS-Fluo-TPP/HA nanogels (Figure S6), which showed that the presence of HGdDOTA within the nanoparticles did not perturb their fluorescent response. As shown above (Figure 3), confocal microscopy images of nanogels confirmed that all the CS-Rhod-TPP/HA or CS-Fluo-TPP/HA NGs were red and green emitters respectively.

Before testing the effectiveness of GdDOTA⊂CS-Rhod-TPP/HA and GdDOTA⊂CS-Fluo-TPP/HA NGs in enhancing the MRI signal, their potential cytotoxicity towards cells, was evaluated by means of MTT and LDH assays (Figure 4) (Fotakis & Timbrel 2006). For that, a murine macrophage cell line (RAW 264.7) was chosen, since macrophages are among the major cells mediating the inflammatory response to foreign substances, especially nanoparticles (Jiang et al. 2017). A20 cells which

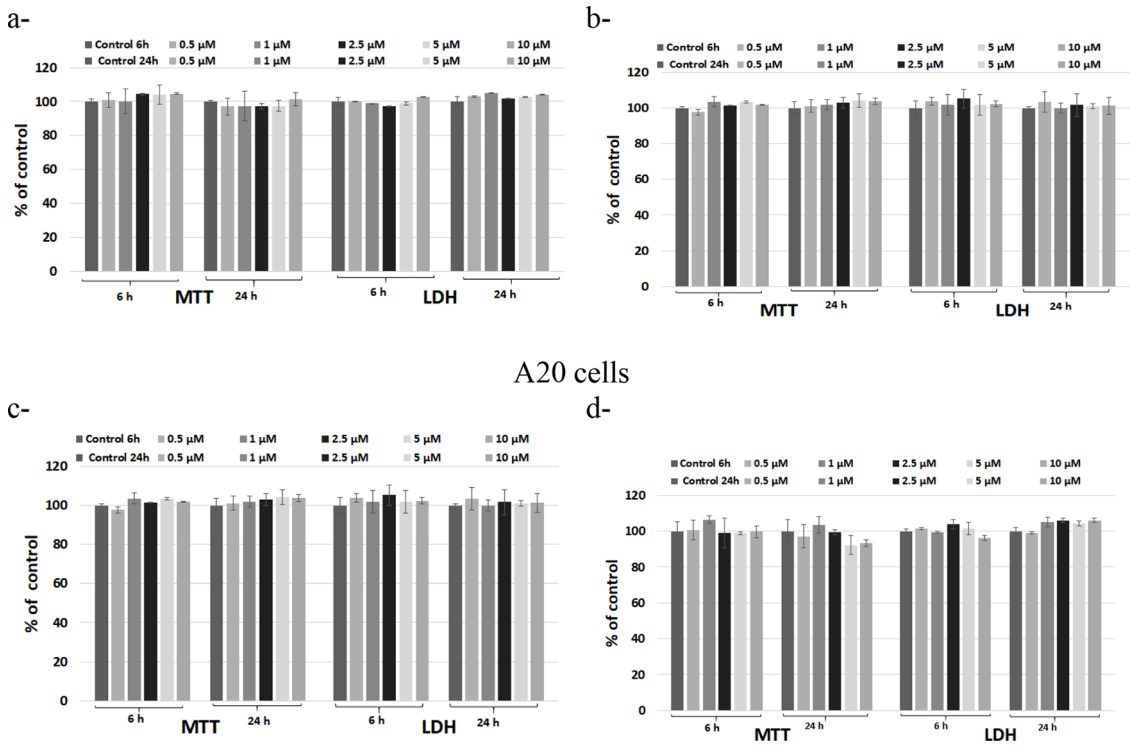

Figure 4. Cell viability and cytotoxicity established by MTT and LDH assays in the presence of RAW 264.7 cells and A20 cells after exposure to 0.5, 1, 2.5, 5 and 10 µM Gd of a and c - GdDOTA⊂CS-Rhod-TPP/HA and b and d- GdDOTA⊂CS-Fluo-TPP/HA NGs for 6 and 24 hours. Results are calculated as means ± sd (n = 3) and expressed as % from controls (untreated cells).

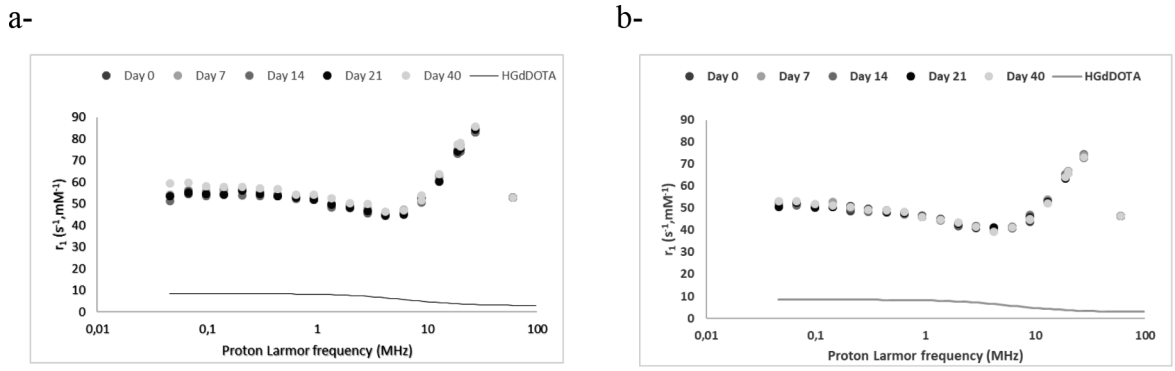

Figure 5. NMRD relaxivity profiles of a- GdDOTA⊂CS-Rhod-TPP/HA NGs and b- GdDOTA⊂CS-Fluo-TPP/HA NGs and their evolution over time (37°C)

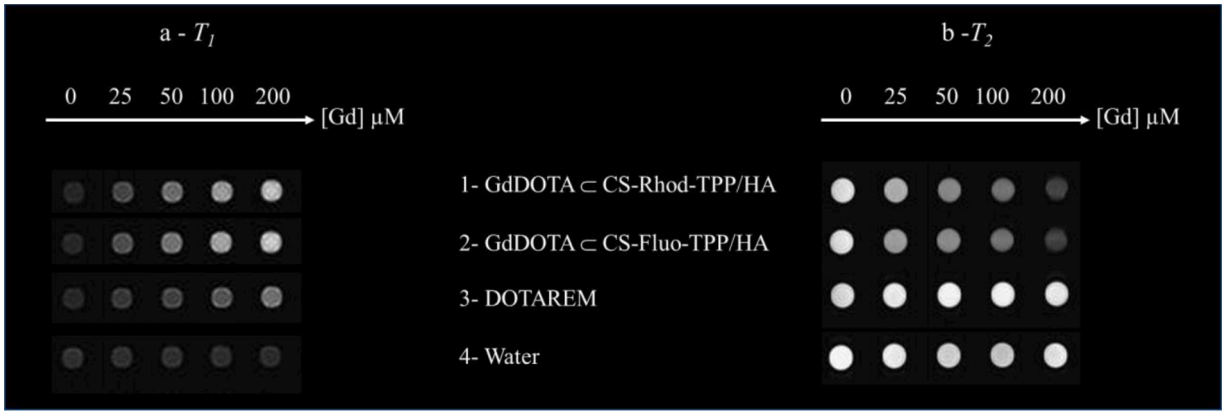

Figure 6. a) T_1- and b) T_2- weighted images of GdDOTA ⊂ CS-Rhod-TPP/HA (line 1) and GdDOTA⊂CS-Fluo-TPP/HA NPs (line 2), DOTAREM® (line 3) and water (line 4) as controls. All samples were imaged at 3T, 37°C with 3D fast spin echo T_1 orT_2 sequences.

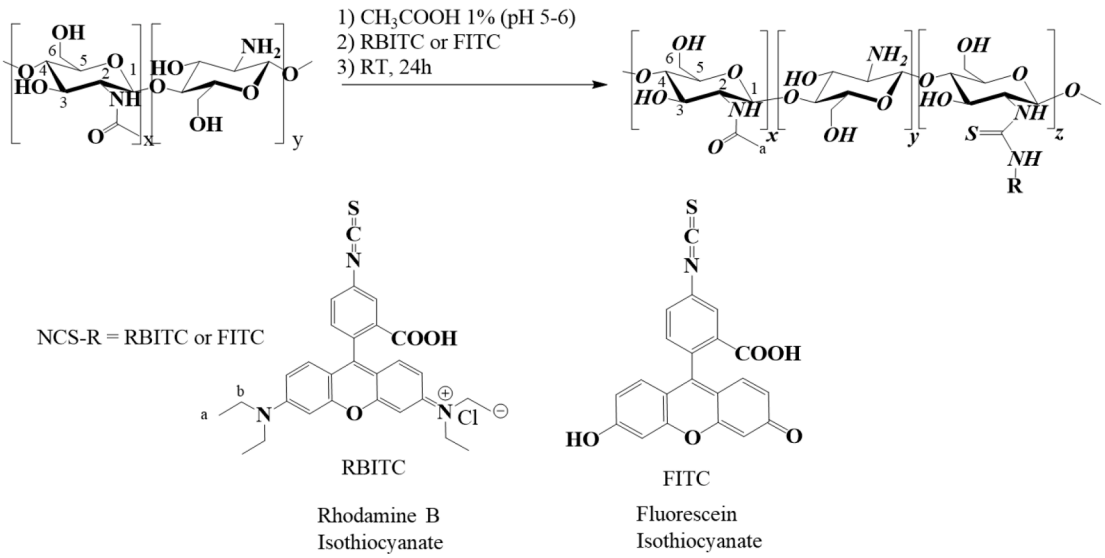

Scheme 1. Syntheses of CS-Rhod and CS-Fluo

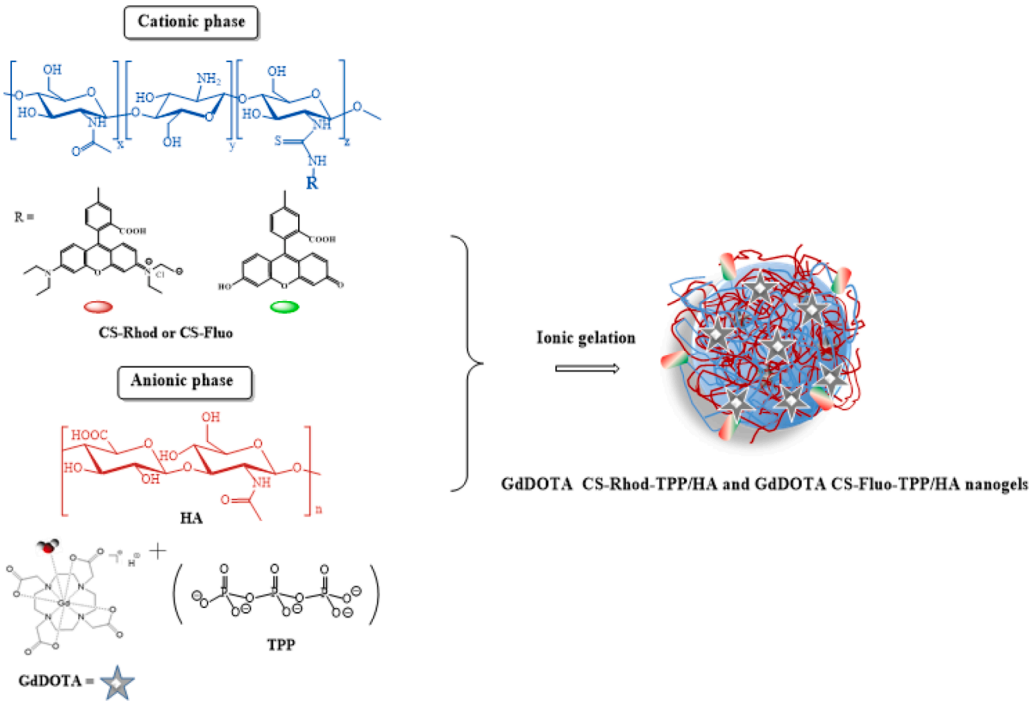

Scheme 2. CS-Rhod-TPP/HA and CS-Fluo-TPP/HA nanogel syntheses

are lymphocyte cells were chosen as they are involved in the immune system (Gheran et al. 2017).

The exposure of RAW264.7 and A20 cells to fluorescent Gd nanogels did not affect the cell survival. Furthermore, this absence of toxicity is similar to the one observed for the non-fluorescent analogues (Gheran et al. 2018, Gheran et al. 2017) which highlighted that fluorophore grafting, while providing additional imaging functionality, did not affect the harmlessness of nanogels to cells.

Finally, in order to evaluate the MRI efficiency of GdDOTA⊂CS-Rhod-TPP/HA and GdDOTA⊂CS-Fluo-TPP/HA NGs, their longitudinal relaxation rates were recorded at 37°C, as a function of resonance frequency. The corresponding NMR dispersion profiles (NMRD) (Figure 5) revealed a maximum in relaxivity between 25 and 30 MHz ($r_1 \geq 80$ $mM^{-1}s^{-1}$) by comparison to GdDOTA relaxivity in the same field region ($r_1 \sim 3.5$ $mM^{-1}s^{-1}$ at 20 MHz) (Idée et al. 2006).

These profiles shapes were typical of Gd chelate with a restricted rotational motion (Merbach, Helm & Toth, 2013). Indeed, the spatial confinement of GdCAs within nanohydrogels allowed to slow-down their tumbling motion. Furthermore, the hydrophilic nature of CS and HA (Basu et al., 2015) that constituted the nanogel polymer matrix allowed the optimization of water residence times in the gadolinium coordination sphere, leading to a strong outer-sphere and/or second-sphere contribution to the relaxivity. Moreover, one should notice that each profile shape was maintained over a period of 40 days (Figure 5), which demonstrated the stability of GdDOTA⊂CS-Rhod-TPP/HA and GdDOTA⊂CS-Fluo-TPP/HA nanogels as well as their ability to contain their Gd loading over the time.

In order to check how this relaxation amplification could be

translated into magnified MR images, T_1- and T_2-weighted images of phantoms containing GdDOTA⊂CS-Rhod-TPP/HA and GdDOTA⊂CS-Fluo-TPP/HA suspensions were acquired on a 3T clinical imager, with DOTAREM® as control (Figure 6).

For the T_1-weighted images, the bright signal enhancement progressively increased with increased gadolinium concentrations in nanogels. Comparison with DOTAREM® control showed that the signal enhancement was due to the incorporation of GdDOTA within the fluorescent CS-TPP/HA nanogels. Indeed, encapsulation of large amounts of GdDOTA in nanogels resulted in an apparent increase in the mass of the complex and then in a restriction of its rotational motion, which was responsible for the exaltation of the relaxivity (Merbach et al. 2013). Conversely for the T_2-weighted images, under the same conditions, image darkening was observed. This important T_2 effect at high magnetic field results from the slow rotation of the encapsulated complexes and/or magnetic susceptibility effects (Aime et al., 2007). As a result, these images corroborated relaxometric measurements and confirmed the dual T_1/T_2 properties of the gadolinium loaded nanogels.

4. Conclusion

In this paper, we reported the synthesis and the characterization of a series of fluorescent chitosans and the subsequent synthesis of biocompatible nanohydrogels by ionic gelation in the presence of hyaluronic acid. MRI and optical imaging modalities were set within the nanogels thanks to chitosan and encapsulation of Gd chelate during the process. The low degree of substitution of chitosans by fluorophores and the hypersensitive MRI character of Gd chelate buried within the nanoparticles allowed to take into account the differences in sensibility between MRI and optical imaging modalities, so as to obtain an optimal signal in both modalities. Both MRI and optical imaging activities were evaluated. T_1 and T_2-weighted phantom MR images of nanogels, recorded on a 3T clinical scanner, showed an increase in image contrast for lesser Gd doses, by comparison to those used with DOTAREM®. The huge content of water and the presence of Gd chelate within the nanogels did not seem to quench their emission. This absence of quenching was demonstrated in fluorescence imaging by their red or green emission. Further work is in progress in order to produce CS-TPP/HA nanohydrogels able to combine multicolor optical coding for multiplexing and magnetic properties.

Declaration of Competing Interest

The authors declare that they have no known competing financial interests or personal relationships that could have appeared to influence the work reported in this paper.

ACKNOWLEDGEGMENTS

Yarong Shi (Bruker Nano, Inc, Santa Barbara, CA 93117, USA and LRN EA4682, University of Reims Champagne Ardenne), Christine Terryn (PICT platform, University of Reims Champagne-Ardenne) and Christophe Portefaix (Radiology Department, CHU de Reims – Hôpital Maison Blanche) are gratefully acknowledged for their help in AFM measurements, optical imaging and MRI experiments respectively.

The authors would like to thank the “Programme de cooperation transfrontalière Interreg France-Wallonie-Vlaanderen” for funding the “Nanocardio” project (http://nanocardio.eu) and the post-doctoral fellowship of V. Malytskyi, the PHC Brancusi program (project n° 43465WA) and the PlAneT platform (supported by the European Regional Development Fund and the Region Champagne Ardenne). This work was also performed with the financial support of the FNRS, FEDER, the ARC, the Walloon Region (Biowin and Interreg projects) and the COST actions. Authors thank the Center for Microscopy and Molecular Imaging (CMMI, supported by European Regional Development Fund Wallonia) and the Bioprofiling platform (supported by the European Regional Development Fund and the Walloon Region, Belgium). Finally, this work was supported by a grant of the Romanian Ministry of Research and Innovation, CCCDI-UEFISCDI, project number PN III-P3-3.1-PM-RO-FR-2019-0204/6BM/2019, within PNCDI III.

Author Contributions

Juliette Moreau* (Polymer syntheses, fluorescent nanogel characterizations – writing original draft), Maite Callewaert* (Nanogel syntheses, characterizations – writing original draft), Volodymyr Malytskyi (Polymer syntheses), Céline Henoumont (DOSY and relaxometry experiments – writing original draft), Sorina N Voicu (Biological assays – writing original draft), Miruna S. Stan (Biological assays), Michael Molinari (AFM measurements supervision – writing), Cyril Cadiou (Polymer and fluorescent nanogels characterizations supervision - Reviewing and editing), Sophie Laurent (NMR supervision of the relaxometry part - reviewing), Françoise Chuburu* (Conceptualization, writing – reviewing and editing).

The manuscript was written through contributions of all authors. All authors have given approval to the final version of the manuscript.

Supplementary materials

Supplementary material associated with this article can be found, in the online version, at doi:10.1016/j.carpta.2021.100104.

References

Aime, S., Delli Castelli, D., Lawson, D., & Terreno, E. (2007). Gd-loaded liposomes as T1, susceptibility, and CEST agents, All in One. *J. Am. Chem. Soc., 129*(9), 2430–2431.

Asberg, P., Nilsson, P., & Inganas, O. (2004). Fluorescence quenching and excitation transfer between semiconducting and metallic organic layers. *J. Appl. Phys., 96*(6), 3140.

Augé, S., Amblard-Blondel, B., & Delsuc, M. A. (1999). Investigation of the diffusion measurement using PFG and tTest r against experimental conditions and parameters. *J. Chim. Phys. Phys.-Chim. Biol., 96*(9–10), 1559–1565.

Basu, A., Kunduru, K. R., Abtew, E. R., & Domb, R. T. (2015). Polysaccharide-Based Conjugates for Biomedical Applications. *Bioconjugate Chem, 26*(8), 1396–1412.

Belabassi, Y., Moreau, J., Gheran, V., Henoumont, C., Robert, A., Callewaert, M., Rigaux, G., Cadiou, C., Vander Elst, L., Laurent, S., Muller, R. N., Dinischiotu, A., Voicu, S. N., & Chuburu, F. (2017). Synthesis and characterization of PEGylated and fluorinated chitosans: application to the synthesis of targeted nanoparticles for drug delivery. *Biomacromolecules, 18*(9), 2756–2766.

Berger, J., Reist, M., Mayer, J. M., Felt, O., Peppas, N. A., & Gurny, R. (2004). Structure and interactions in covalently and ionically crosslinked chitosan hydrogels for biomedical applications. *Eur. J. Pharm. Biopharm., 57*, 19–34.

Callewaert, M., Roullin, V. G., Cadiou, C., Millart, E., Van Gulik, L., Andry, M. C., Portefaix, C., Hoeffel, C., Laurent, S., Vander Elst, L., Muller, R., Molinari, M., & Chuburu, F. (2014). Tuning the composition of biocompatible Gd nanohydrogels to achieve hypersensitive dual T1/T2 MRI contrast agents. *J. Mater. Chem. B, 2*(37), 6397–6405.

Courant, T., Roullin, V. G., Cadiou, C., Callewaert, M., Andry, M. C., Portefaix, C., Hoeffel, C., de Goltstein, M. C., Port, M., Laurent, S., Vander Elst, L., Muller, R., Molinari, M., & Chuburu, F. (2012). Hydrogels Incorporating GdDOTA: Towards Highly Efficient Dual T1/T2 MRI Contrast Agents. *Angew. Chem., Int. Ed. Engl., 51*(36), 9119–9122.

Fotakis, G., & Timbrell, J. A. (2006). In vitro cytotoxicity assays: Comparison of LDH, neutral red, MTT and protein assay in hepatoma cell lines following exposure to cadmium chloride. *Toxicol. Lett., 160*, 171–177.

Gheran, C. V., Voicu, S. N., Rigaux, G., Callewaert, M., Chuburu, F., & Dinischiotu, A. (2017). Biological effects induced by Gadolinium nanoparticles on Lymphocyte A20 cell line. *The EuroBiotech Journal, 1*, 57–64.

Gheran, C. V., Rigaux, G., Callewaert, M., Berquand, A., Molinari, M., Chuburu, F., Voicu, S. N., & Dinischiotu, A. (2018). Biocompatibility of Gd-Loaded Chitosan-Hyaluronic Acid Nanogels as Contrast Agents for Magnetic Resonance Cancer Imaging. *Nanomaterials, 8*(4), 201.

Gianolio, E., Bardini, P., Arena, F., Stefania, R., Di Gregorio, E., Iani, R., & Aime, S. (2017). Gadolinium retention in the rat brain: assessment of the amounts of insoluble gadoliunium-containing species and intact gadolinium complexes after repeated administration of gadolinium-based contrast agents. *Radiology, 285*(3), 839–849.

Gupta, A., Caravan, P., Price, W. S., Platas-Iglesias, C., & Gale, E. M. (2020). Applications for transition-metal chemistry in contrast-enhanced magnetic resonance imaging. *Inorg. Chem., 59*, 6648–6678.

Gupta, K. C., & Jabrail, F. H. (2006). Preparation and characterization of sodium hexameta phosphate cross-linked chitosan microspheres for controlled and sustained delivery of centchroman. *Int. J. Biol. Macromol., 38*, 272–283.

Hirai, A., Odani, H., & Nakajima, A (1991). Determination of Degree of Deacetylation of Chitosan by H NMR Spectroscopy. *Polymer. Bulletin, 26*(1), 87–94.
Idée, J. M., Port, M., Raynal, I., Schaefer, M., Le Greneur, S., & Corot, C. (2006). *Fundamental & Clinical Pharmacology, 20*, 563–576.
Johnson, C. S., Jr. (1999). Diffusion Ordered Nuclear Magnetic Resonance Spectroscopy: Principles and Applications. *Prog. Nucl. Magn. Reson. Spectrosc, 34*(3–4), 203–256.
Jiang, L. Q., Wang, T. Y., Webster, T. J., Duan, H. J., Qiu, J. Y., Zhao, Z. M., & Zheng, C. L. (2017). Intracellular disposition of chitosan nanoparticles in macrophages: intracellular uptake, exocytosis, and intercellular transport. *Int. J. Nanomed., 12*, 6383–6388.
Kanda, T., Oba, H., Toyoda, K., Kitajima, K., & Furui, S. (2016). Brain gadolinium deposition after administration of gadolinium-based contrast agents. *Jpn. J. Radiol., 34*, 3–9.
Khawaja, A. Z., Cassidy, D. B., Al Shakarchi, J., McGrogan, D. G., Inston, N. G., & Jones, R. G (2015). Revisiting the risks of MRI with Gadolinium based contrast agents—review of literature and guidelines. *Insights Imaging, 6*, 553–558.
Leng, T., Jakubek, Z. J., Mazloumi, M., Leung, A. C. W., & Johnston, L. J. (2017). Ensemble and Single Particle Fluorescence Characterization of Dye-Labeled Cellulose Nanocrystals. *Langmuir, 33*(32), 8002–8011.
Lux, J., Chan, M., Van der Elst, L., Schopf, E., Mahmoudi, S., Laurent, S., & Almutairi, A. (2013). Metal chelating crosslinkers form nanogels with high chelation stability. *J. Mater. Chem. B., 1*, 6359. -6354.
Ma, O., Lavertu, M., Sun, J., Nguyen, S., Buschmann, M. D., Winni, F. M., & Hoemann, C. D. (2008). Precise derivatization of structurally distinct chitosans with rhodamine B isothiocyanate. *Carbohydr. Polym., 72*(4), 616–624.
Mei, S., Zhou, J., Sun, H-T., Cai, Y., Sun, L-D., Jun, D., & Yan, C-H. (2021). Networking state of ytterbium ions probing the origin of luminescence quenching and activation in nanocrystals. *Adv. Sci., 8*(6), Article 2003325.
Merbach, A. E., Helm, L., & Toth, E. (2013). *The Chemistry of Contrast Agents in Medical Magnetic Resonance Imaging* (2nd Ed.). Chichester: Wiley and Sons.
Rigaux, G., Gheran, C. V., Callewaert, M., Cadiou, C., Voicu, S. N., Dinischiotu, A., Andry, M. C., Vander Elst, L., Laurent, S., Muller, R. N., Berquand, A., Molinari, M., Huclier-Markai, S., & Chuburu, F. (2017). A multi-technique approach combining DLS, AF4 and AFM in liquid mode to select Gd-loaded chitosan-TPP nanohydrogels for MRI positive contrast agent for Lymph Node Imaging. *Nanotechnology, 28*, Article 055705. Article ID.
Rogosnitzky, M., & Branch, S. (2016). Gadolinium-based contrast agent toxicity: a review of known and proposed mechanisms. *Biometals, 29*(3), 365–376.
Sang, Z., Quan, J., Han, J., Deng, X., Shen, J., Li, G., & Xie, Y. (2020). Comparison of three water-soluble polyphosphate tripolyphosphate, phytic acid, and sodium hexametaphosphate as crosslinking agents in chitosan nanoparticle formulation. *Carbohydrate Polymers, 230*, Article 115577.
Sinagaglia, G., Magro, M., Miotto, G., Cardillo, S., Agostinelli, E., Zboril, R., Bidollari, E., & Vianello, F. (2012). Catalytically active bovine serum amine oxidase bound to fluorescent and magnetically drivable nanoparticles. *Int. J. Nanomed., 7*, 2249–2259.
Soleimani, A., Martinez, F., Economopoulos, V., Foster, P. J., Scholl, T. J., & Gillies, E. R. (2013). Polymer cross-linking: a nanogel approach to enhancing the relaxivity of MRI contrast agents. *J. Mater. Chem. B., 1*, 1027–1034.
Vårum, K. M., Antohonsen, M. W., Grasdalen, H., & Smidsrød, O (1991). Determination of the Degree of N-Acetylation and the Distribution of N-Acetyl Groups in Partially N-Deacetylated Chitins (Chitosans) by High-Field NMR Spectroscopy. *Carbohydr. Res., 211*, 17–23.
Washner, J., Gael, E. M., Rodriguez-Rodriguez, A., & Caravan, P. (2019). Chemistry of MRI contrast agents: current challenges and new frontiers. *Chem. Rev., 119*, 957–1057.
Xia, S., Yang, H., Duan, L., Gao, G. H., & Zhang, X. (2016). A potential dual-modality optical imaging probe based on the pH-responsive micelle. *J. Polym. Res., 23*, 179.